Journal of Power Sources 215 (2012) 240–247

Contents lists available at SciVerse ScienceDirect

Journal of Power Sources

journal homepage: www.elsevier.com/locate/jpowsour

The stability of organic solvents and carbon electrode in nonaqueous Li-O_2 batteries

Wu Xu [a,*], Jianzhi Hu [b], Mark H. Engelhard [c], Silas A. Towne [a], John S. Hardy [a], Jie Xiao [a], Ju Feng [b], Mary Y. Hu [c], Jian Zhang [a], Fei Ding [a,d], Mark E. Gross [a], Ji-Guang Zhang [a,**]

[a] Energy and Environment Directorate, Pacific Northwest National Laboratory, Richland, WA 99354, United States
[b] Fundamental and Computational Sciences Directorate, Pacific Northwest National Laboratory, Richland, WA 99354, United States
[c] Environmental and Molecular Sciences Laboratory, Pacific Northwest National Laboratory, Richland, WA 99354, USA
[d] National Key Lab of Power Sources, Tianjin Institute of Power Sources, Tianjin 300381, PR China

HIGHLIGHTS

- Discharge products from six types of aprotic organic solvents were investigated.
- The amount of Li_2O_2 formed during discharge strongly depends on solvent systems.
- Glyme-based electrolytes result in more Li_2O_2 formation during discharge.
- All tested carbon air electrodes contain Li_2CO_3.
- Li_2CO_3 is formed from the decomposition of solvent, not carbon electrode.

ARTICLE INFO

Article history:
Received 24 March 2012
Received in revised form
7 May 2012
Accepted 10 May 2012
Available online 18 May 2012

Keywords:
Li-O_2 battery
Lithium peroxide
Electrolyte
Organic solvent
Discharge product

ABSTRACT

The effects of six types of aprotic organic solvents on the discharge performance and discharge products in Li-O_2 batteries are systematically investigated. A large amount of Li_2O_2 is identified in the air electrodes discharged in glyme-based electrolytes, while only a small amount of Li_2O_2 is detected in the air electrodes discharged in the electrolytes of nitrile, ionic liquid, phosphate, and sulfoxide. Li_2CO_3 and LiF are also found as byproducts whose compositions are related to the solvents. Li_2CO_3 is produced from oxidation and decomposition of the solvent, not from the oxidation of the carbon-based air electrode, as revealed by using a ^{13}C-labeled carbon electrode and the solid-state ^{13}C-magic angle spinning nuclear magnetic resonance technique. LiF in the discharge products can be attributed to the attack of superoxide radical anions to the Teflon binder and/or the F-containing imide salt. The formation of these byproducts will significantly reduce the Coulombic efficiency and cycle life of the Li-air batteries. Among the studied solvents, dibutyl diglyme is the suitable solvent for Li-O_2 batteries based on its overall properties. However, better electrolytes that can ensure the formation of Li_2O_2 but minimize other reaction products need to be further investigated for long cycling rechargeable Li-air batteries.

1. Introduction

Li-O_2 or Li-air batteries have attracted much attention in recent years because of their ultra-high theoretical specific energies of 11 kWh kg^{-1} based on the lithium electrode alone or about 5.2 kWh kg^{-1} when the oxygen weight is included [1–3]. It is expected that a practical Li-air battery can have an energy density of more than 800 Wh kg^{-1}, which far exceeds those of the state-of-the-art lithium ion batteries (~200 W h Kg^{-1}) widely used in commercial electronics and electric vehicles today. A practical specific energy of 362 W h kg^{-1} has been reported by Zhang et al. for a Li-air battery with a nonaqueous electrolyte in a pouch configuration [4]. However, the reversibility of Li-O_2 batteries is still far from being satisfactory, with a cycle life ranging from several to 100 cycles depending on catalysts and electrolyte compositions [5–13]. The electrolytes used in these Li-O_2 batteries contained primarily organic carbonate esters as solvent systems because of their success in Li-ion batteries.

The limited cycle life of Li-O_2 batteries with carbonate-based electrolytes is mainly due to the side reactions between oxygen and electrolyte during the discharge process, which produces

* Corresponding author. Tel.: +1 509 375 6934; fax: +1 509 375 3864.
** Corresponding author. Tel.: +1 509 372 6515; fax: +1 509 375 3864.
E-mail addresses: wu.xu@pnnl.gov (W. Xu), jiguang.zhang@pnnl.gov (J.-G. Zhang).

0378-7753/$ – see front matter © 2012 Elsevier B.V. All rights reserved.
doi:10.1016/j.jpowsour.2012.05.021

irreversible organic and inorganic carbonate species (i.e., lithium alkylcarbonates and Li_2CO_3) rather than the reversible Li_2O_2. These discharge byproducts result from the reduction of carbonate-based solvent molecules [12–17]. To address this non-sustainable process, Bruce and co-workers [16] and we [17] separately proposed chemical reaction mechanisms that occur during the discharge and charge processes of a Li-O_2 battery in an organic carbonate electrolyte. During the discharge step, organic and inorganic carbonate species are formed by reductive decomposition of organic carbonate solvent molecules that react with superoxide radical anions ($O_2^{\bullet-}$) formed through single-electron reduction of oxygen. During the charge step, lithium alkylcarbonates undergo oxidative decomposition and release CO_2, CO, and other gases. These conclusions are supported by the results of *ex situ* x-ray diffraction (XRD) [12–17], Fourier-transform infrared (FTIR) spectroscopy 12,13,16], and solid-state nuclear magnetic resonance (NMR) analyses [16] on the chemical products formed during discharging, and the results of *in situ* gas chromatography/mass spectroscopy (GC/MS) [14,17] and differential electrochemical mass spectroscopy (DEMS) [15,16] on the gases formed during charging. Therefore, a stable electrolyte that does not lead to irreversible byproduct formation during the discharge and charge processes is needed for a fully reversible Li-O_2 battery.

Recently, Abraham and co-workers reported the influence of organic solvents on the oxygen reduction reaction in nonaqueous electrolytes [18]. They studied four different solvents, dimethyl sulfoxide (DMSO), acetonitrile (MeCN), dimethoxyethane (DME), and tetraethylene glycol dimethyl ether (TEGDME), with a range of donor numbers and found that the solvent and the supporting electrolyte cations significantly affect the reduction products and their reversibility. They also reported the formation of Li_2O_2 during discharge in an electrolyte of $LiPF_6$ in TEGDME and a limited cycle life of a Li-O_2 cell using this electrolyte with no catalyst in the air electrode [19]. McCloskey et al. [15] also reported the formation of Li_2O_2 from DME electrolyte. However, most of the analysis in references 18 and 19 was based on electrochemical test data, and no thorough analyses of other reaction products were undertaken. More direct analyses should be undertaken to verify the reaction products formed in different electrolytes and to confirm the effect of these electrolytes on the battery performance.

In this paper, we report the results of our recent study on the effects of different types of aprotic organic solvents on the formation of discharge products in Li-O_2 batteries. The aprotic solvents were selected from ethers or glymes, sulfoxides, phosphates, nitriles with long chains (for being stable with Li metal) and ionic liquids for this study, and compared with carbonate solvents. Ketones, lactones and carboxylate esters were not studied because all of them have −C(=O)− group in the molecular moiety as the carbonate solvents have, which makes the solvent molecules unstable against superoxide radical anion and its related species. Li-O_2 batteries using these electrolytes were assembled and discharged under similar conditions. The reaction products formed in the carbon-based air electrodes during the discharge process were systematically analyzed using various techniques, including XRD, X-ray photoelectron spectroscopy (XPS), GC/MS, and solid-state ^{13}C-magic angle spinning (MAS) nuclear magnetic resonance (NMR) spectroscopy. The effects of these reaction products on the cyclability of Li-air batteries will also be discussed.

2. Experimental

2.1. Preparation and cell testing

Ethylene carbonate (EC), propylene carbonate (PC), DME, tri(ethylene glycol) dimethyl ether (i.e., Triglyme), di(ethylene glycol) di-n-butyl ether (i.e. butyl diglyme, BDG), and lithium bis(trifluoromethylsulfonyl)imide (LiTFSI) (all in battery grade) were purchased from Novolyte Technologies. DMSO, triethyl phosphate (TEPa), 1-butyl-1-methylpyrrolidium bis(trifluoromethylsulfonyl)imide (Pyr14TFSI), and 4A molecular sieves were ordered from Sigma–Aldrich. Sebaconitrile was bought from Acros Organics. Lithium foil (99.9%, 0.75-mm thick) was obtained from Alfa Aesar®. All non-battery-grade solvents were dried with excess pre-dried 4A molecular sieves for several days before use. Electrolytes of 1 M LiTFSI in different solvents were prepared inside an MBraun glove box filled with purified argon and in which the moisture and oxygen content was less than 1 ppm.

The Ketjen black (KB) carbon-based air electrodes were prepared as described previously [20]. DuPont™ Teflon® PTFE-TE3859 fluoropolymer resin was used as a binder, and the weight ratio of carbon:Teflon after drying was 85:15. The KB carbon loading in the final electrode was controlled at about 15.1 mg cm^{-2}, and the KB-air electrode disks had a diameter of 1.59 cm and an area of 1.98 cm^2.

The coin-cell-type Li-O_2 batteries of 2325 size were assembled inside the MBraun glove box as described in previously published papers [3,21]. The 2325 coin cell kits were purchased from National Research Council Canada (CNRC), and the cell pans were machine-drilled with nineteen φ1.0 mm holes in an evenly distributed pattern to allow oxygen access. The cells were constructed by layering, in sequence, the following components: an air electrode disk on the cell pan, a piece of separator material (2.06-cm diameter, Whatman® GF/D glass microfiber filter paper), 280 μL of electrolyte, a lithium disk (1.59 cm diameter), a stainless steel spacer (0.5 mm thick, from Pred Materials), and a coin cell cover with a polypropylene gasket. The whole assembly was crimped at a gas pressure of 200 psi using a pneumatic coin cell crimper purchased from CNRC. The excess electrolyte was drained out from the cells through the O_2 diffusion windows during crimping.

Each Li-O_2 coin-cell battery was placed in an individual 226 cm^3 Teflon container which was filled with purified oxygen at a pressure of about 1 atm. The batteries were discharged at room temperature on an Arbin Instruments BT-2000 battery tester at a constant current density of 0.05 mA cm^{-2} to 2.0 V and then under a constant voltage until the current density decreased to $\leq$0.01 mA cm^{-2}. After discharging, the Li-O_2 coin cells were disassembled in the glove box, and the air electrodes were washed thoroughly several times by immersion in fresh anhydrous DME for at least 1 h each time. After washing, the cells were dried overnight under vacuum at room temperature.

2.2. Measurements and characterization

The viscosity, ionic conductivity and dissolved oxygen of the electrolytes were measured using the methods and instruments reported previously [21]. Prior to the measurement of dissolved oxygen, the electrolyte samples were put inside a dry box purged continuously with compressed air (a relative humidity of $< 1\%$) overnight in order to saturate the electrolytes with air.

Analysis of the gas evolution of KB-based air electrodes with different electrolytes during charging was conducted as described in previously published papers [14,17]. The Teflon container holding the cell after discharging in oxygen was connected to a GC/MS instrument. The Teflon container was evacuated and refilled with purified argon at a flow rate of 50 cm^3 min^{-1}. The evacuation and refilling cycle were conducted three times, followed by purging the container with argon for several hours at a flow rate of 3 cm^3 min^{-1}. The cell was charged on a CHI 660C electrochemical workstation from the open circuit potential to 4.5 V at a constant current rate of C/10 where 1 C was the discharge capacity of the cell. The gases generated were analyzed in real time using GC/MS.

XRD patterns of the discharged air electrodes were measured in a D8 Advance x-ray diffractometer (Bruker AXS, Inc., Madison, Wisconsin) equipped with an HTK 1200 atm-controlled chamber (Anton Paar, Ashland, Virginia) and a VANTEC-1 position sensitive x-ray detector (Bruker AXS). Measurements were performed at room temperature under nitrogen atmosphere from 10 to 80° 2Θ with 0.007° 2Θ steps and at least 320.8 s of total count time per step.

XPS measurements of the discharged air electrodes were performed with a Physical Electronics Quantera Scanning X-ray Microprobe. The samples were mounted onto the standard Physical Electronics 75 mm × 75 mm sample holder using 2-56 stainless steel screws inside a nitrogen recirculated glove box operated at<0.2 ppm O_2 and a dew point of −80 °C. Then the sample holder was placed into the XPS vacuum introduction system and pumped to $< 1 \times 10^{-7}$ Torr using a turbomolecular pumping system prior to introduction into the main ultra-high vacuum system. The main vacuum system pressure was maintained at $<5 \times 10^{-9}$ Torr during analysis and pumped using a series of sputter ion pumps and turbomolecular pumps. This XPS system used a focused monochromatic Al Kα X-ray (1486.7 eV) source for excitation and a spherical section analyzer. The instrument had a 32 element multichannel detection system. A 200 μm diameter focused X-ray spot was used for the analysis. The X-ray beam was incident normal to the sample and the photoelectron detector was at 45° off-normal. High energy resolution spectra were collected using a pass-energy of 69.0 eV with a step size of 0.125 eV. For the Ag 3d5/2 line, these conditions produced a full width half maximum (FWHM) of 0.91 eV. Specimen charging was minimized by flooding the sample with low energy electrons at ∼1 eV, 20 μA and low energy Ar^+ ions.

^{13}C single pulse MAS NMR experiments were performed on a 500 MHz Varian NMR System, corresponding to ^1H and ^{13}C Larmor frequencies of 499.835 and 125.687 MHz, respectively. A commercial cross-polarization/MAS probe with a 4 mm outside-diameter, pencil-type spinner system was used. The sample spinning rate used for all measurements was about 14 kHz. Tetrakis(trimethylsilyl) silane (TKS), $[(CH_3)_3Si]_4Si$, was used as a secondary reference for ^{13}C (3.5 ppm) relative to trimethylsilane (TMS) $(CH_3)_4Si$ (0 ppm) [22]. The pulse angle for acquiring ^{13}C spectra was approximately 45°. The recycle time used was 50 s, with a total accumulation number of approximately 2000 for acquiring each spectrum. The weight of each electrode material was about 30–40 mg. All spectra were acquired at room temperature. Quantitative peak areas for the Li_2CO_3 peak in the ^{13}C MAS NMR spectra of various samples were obtained using the following strategy. The weight of the samples loaded into the MAS rotor for each sample was recorded during sample loading. The matching and tuning conditions of the RF circuit of the NMR probe were set as the same as possible using a network analyzer. All other experimental conditions were kept identical from sample to sample. In this way, the absolute peak area against the spectrometer standard is directly proportional to the sample weight and the number of accumulation numbers. The absolute peak area for the Li_2CO_3 peak was obtained by simulating the spectrum of each sample using NutsPro (Acorn NMR, 1993–1997), a commercially available software package. The peak area obtained from NutsPro was then normalized based on per unit weight of samples and per unit number of accumulation numbers. The normalized peak area can then be quantitatively compared between the samples because the normalized peak area is proportional to the amount of the Li_2CO_3 product in the electrode materials.

3. Results and discussion

3.1. Electrolyte properties and discharge performance

Considering the reactivity of lithium metal to protic organic solvents and the open nature of Li-O_2 or Li-air battery systems, the solvents for this study were chosen from aprotic organic liquid compounds with relatively high boiling points (e.g., >180 °C) to reduce solvent loss via evaporation through the oxygen diffusion holes on the battery case. LiTFSI was chosen as the solute because it has better stability against moisture and heat than $LiPF_6$. Table 1 lists the room temperature values of viscosity, ionic conductivity, and dissolved oxygen of the 1.0 M LiTFSI electrolytes with the chosen solvent systems. The oxygen solubility data measured with the Oakton 650 Series multiparameter meter were slightly lower than the actual values as commented by Ein-Eli and Kraytsberg [23], but they are listed in Table 1 just for a relative comparison. Fig. 1 shows the discharge profiles as a function of discharge capacity of Li-O_2 batteries using different electrolytes at a discharge current of 0.05 mA cm^{-2}, and the discharge capacity data are listed in Table 1 for easy comparison. The discharge performance of the ionic liquid Pyr14TFSI at 0.02 mA cm^{-2} also is included in Fig. 1 for comparison. The upward spikes on the discharge curves of DMSO and Pyr14TFSI (at 0.02 mA cm^{-2}) were caused by a power outage that occurred during testing.

Fig. 1 shows that, when the cells were discharged to 2.0 V at the same current density (0.05 mA cm^{-2}), the discharge capacities based on the KB carbon weight (in decreasing order and without including the constant voltage discharge stage) of Li-O_2 cells using each solvent system are in the following order: DMSO (1275 mAh g^{-1}) > BDG (1215 mAh g^{-1}) >> PC-EC (876 mAh g^{-1}) > Sebaconitrile (823 mAh g^{-1}) > Triglyme (654 mAh g^{-1}) > TEPa (400 mAh g^{-1}) >> Pyr14TFSI (17 mAh g^{-1}). However, when the constant voltage discharge stage is counted, the cell using BDG solvent shows a higher capacity than that of DMSO, i.e. 1324 mAh g^{-1} vs. 1279 mAh g^{-1}. On the other hand, the cell voltage decreases in the following order: 1) DMSO ∼ PC-EC (2.9 V), 2) Sebaconitrile (2.8 V), 3) BDG ∼ Triglyme (2.7 V), 4) TEPa (2.68 V), and 5) Pyr14TFSI (2.6 V). The discharge performance is mainly related to the combined effects of viscosity, ionic conductivity, oxygen solubility, and other characteristics (e.g., the wettability on the air electrode) of each electrolyte, as discussed in our previous reports [3,21]. The discharge capacity of the cells using ionic liquid Pyr14TFSI was very poor when discharged at 0.05 mA cm^{-2}, but it could reach 1031 mAh g^{-1} at 0.02 mA cm^{-2}, indicating that such ionic liquids can only be discharged at very low current rates.

3.2. Identification of discharged products

Fig. 2 shows the XRD patterns of the KB-air electrodes discharged to 2.0 V in different electrolytes in an oxygen atmosphere, compared with Li_2O_2, Li_2CO_3, LiF and Teflon serving as standard references. It is shown that characteristic XRD peaks for Li_2O_2 appear clearly for the electrodes discharged in electrolytes containing Triglyme and BDG, but not apparent for the electrodes discharged in other solvent-based electrolytes. This means that Triglyme and BDG (both are actually glymes or di-ethers) can lead

Table 1
Physical properties of electrolytes of 1.0 M LiTFSI in different organic solvents at ca. 25 °C and capacities of the Li-O_2 cells with such electrolytes discharged to 2.0 V at 0.05 mA cm^{-2}.

Solvent	Viscosity (cP)	Conductivity (mS cm^{-1})	Dissolved O_2 (mg L^{-1})	Capacity (mAh g^{-1} C)
PC-EC (1:1 wt)	7.1	5.04	5.68	876
Triglyme	7.4	4.01	7.25	654
BDG	12.4	2.53	9.97	1215
DMSO	5.4	18.27	6.17	1275
TEPa	16.2	3.80	7.45	400
Sebaconitrile	45.8	0.87	3.86	823
Pyr14TFSI	523.1	0.49	1.78	17

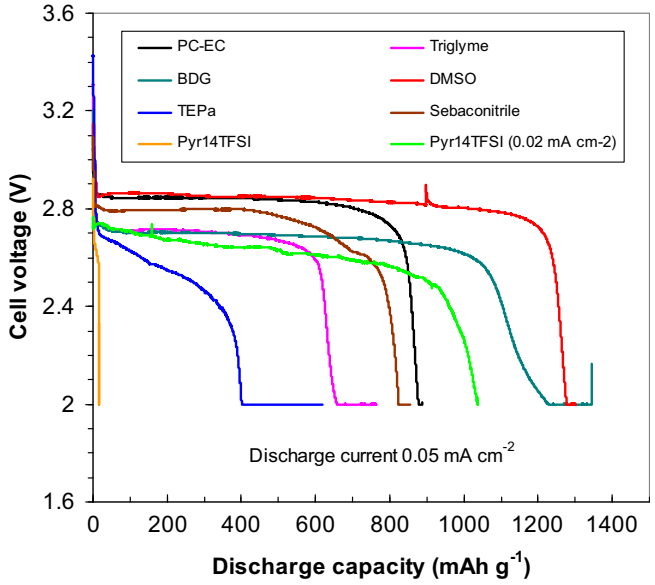

Fig. 1. Comparison of the discharge voltage profiles as a function of discharge capacity for Li-O_2 batteries using different electrolytes. All cells were tested in a pure oxygen environment.

to the formation of the desired Li_2O_2 in good crystalline structure. This is probably because ethers and glymes are relatively stable to superoxide radical anion ($O_2^{\bullet-}$) which is the single-electron reduction species of oxygen formed during discharge [18,19]. As for other solvent systems, there is either no Li_2O_2 formed in the air electrodes or a small amount of poorly crystallized Li_2O_2 generated which cannot be detected by XRD, which should be confirmed by other techniques.

The discharged air electrodes were also tested by Fourier transform infrared spectroscopy (FTIR). However, the signals were very weak due to the strong absorption of lights by the dark black KB-carbon materials in each electrode and no meaningful information can be obtained. Therefore, the XPS technique was used to further analyze the discharged air electrodes because XPS can tell the elements and bonding conditions of the compounds in the surface layers of the tested samples. Fig. 3 shows the XPS results of

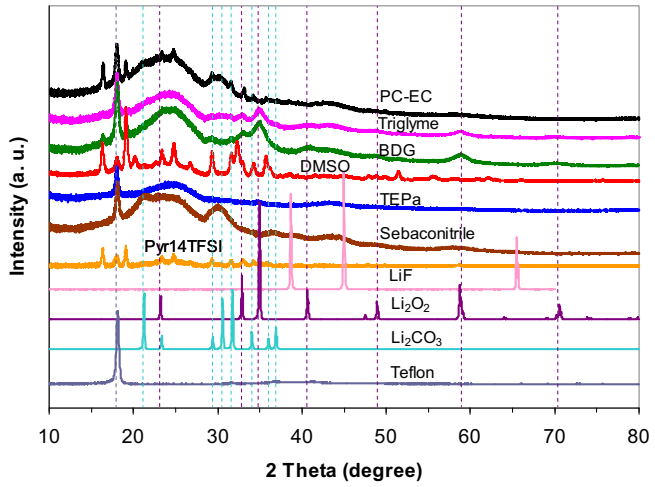

Fig. 2. XRD patterns of the KB-air electrodes discharged to 2.0 V in different electrolytes in an oxygen atmosphere, compared with Li_2O_2, Li_2CO_3, LiF and Teflon serving as standard references.

the discharged KB-air electrodes in terms of (a) Li1s, (b) C1s, (c) O1s, (d) F1s. In the air electrode discharged in PC-EC based electrolyte the major products are Li_2CO_3 and LiF and scarce Li_2O_2 is identified, which is consistent with the literature reports [12–17]. As for the air electrode discharged in Triglyme, the inorganic products are mainly Li_2O_2 and Li_2CO_3 with a trace amount of LiF. From the air electrode discharged in BDG, the main product is Li_2O_2, with some LiF and a trace amount of Li_2CO_3. From the air electrode discharged in DMSO, a significant amount of LiF is formed as well as some unknown oxygen-containing species, but not much Li_2O_2 and Li_2CO_3 can be identified. From the air electrode discharged in TEPa, the discharged products are mostly Li_2CO_3, some Li_2O_2 and a very small amount of LiF. From the air electrode discharged in Sebaconitrile and Pyr14TFSI, the compounds formed are Li_2O_2, LiF, Li_2CO_3 and some unidentified oxygen-containing species. This demonstrates that the solvent system strongly affects the discharged products and their compositions. LiF formation in different contents in all of the air electrodes is probably due to the decomposition of the lithium salt LiTFSI that has a formula of $LiN(SO_2CF_3)_2$ and/or the decomposition of the binder PTFE by the attack of the superoxide radical anion. The real reasons are currently under investigation. The absence of LiF characteristic peaks in the XRD plots in Fig. 2 indicates that the LiF formed during discharge is most likely in poor crystallinity.

In Fig. 3(c), the O1s peaks at ca. 528.0 eV in BDG sample and 532.8 eV in DMSO, Sebaconitrile and Pyr14TFSI samples cannot be identified at this time. In addition, the small or nearly no peaks of F1s for LiF in Fig. 3(d) are found for air electrodes discharged in Triglyme and TEPa. Similarly, the F1s peaks for $-(CF_2-CF_2)-$ are not detected in the electrode discharged in DMSO and Sebaconitrile based electrolytes. This is probably because the XPS technique can only detect a very small area of several square micrometers each time. The non-uniformly formed discharge products at the surface of the air electrode will cause such big contrast.

To further investigate the possible formation of Li_2O_2 which is not detected by XRD and XPS techniques due to their poor crystallinity or non-uniform distribution, the in-situ GC/MS method was used to analyze the gas formation and composition during the charge process of Li-O_2 cells after they were first discharged in different electrolytes. The compositions of the selected gases and the charge voltage profiles as a function of time for the air electrodes discharged in different solvent systems are shown in Fig. 4(a)–(g). The gas compositions were calculated based on the total gas amount including the carrier gas (helium, but it is not shown in the figures). The continuous detection of O_2 even after the charging process was stopped, as shown in Fig. 4, because the container had a large volume and it took some time to purge out the O_2 that was generated and was still in the container.

It is found from Fig. 4 that there was nearly no oxygen released from the cell that was discharged in electrolyte containing PC-EC, but all other six cells released different amounts of O_2. The O_2 composition in the gases released during charging is about 0.038% for BDG, 0.023% for Triglyme, 0.022% for TEPa and Sebaconitrile, and 0.010% for DMSO and Pyr14TFSI. It seems that there is no big difference in the O_2 evolution curve with test time among these solvent systems. However, when counting the total amount of O_2 released during the charging process, the following order is obtained for the tested solvent systems from high to low: BDG >> Sebaconitrile > Triglyme > DMSO ~ TEPa >> Pyr14TFSI > PC-EC. For simple analysis, we assume that all released O_2 is from the decomposition of Li_2O_2 in the discharged air electrode, then the first cycle efficiency of charge capacity over discharge capacity for the studied solvent systems is about 30.7% for BDG, 17.4% for Triglyme, 16.1% for Sebaconitrile, 11.6% for Pyr14TFSI, 9.6% for DMSO and TEPa, and 2.2% for PC-EC. The poor

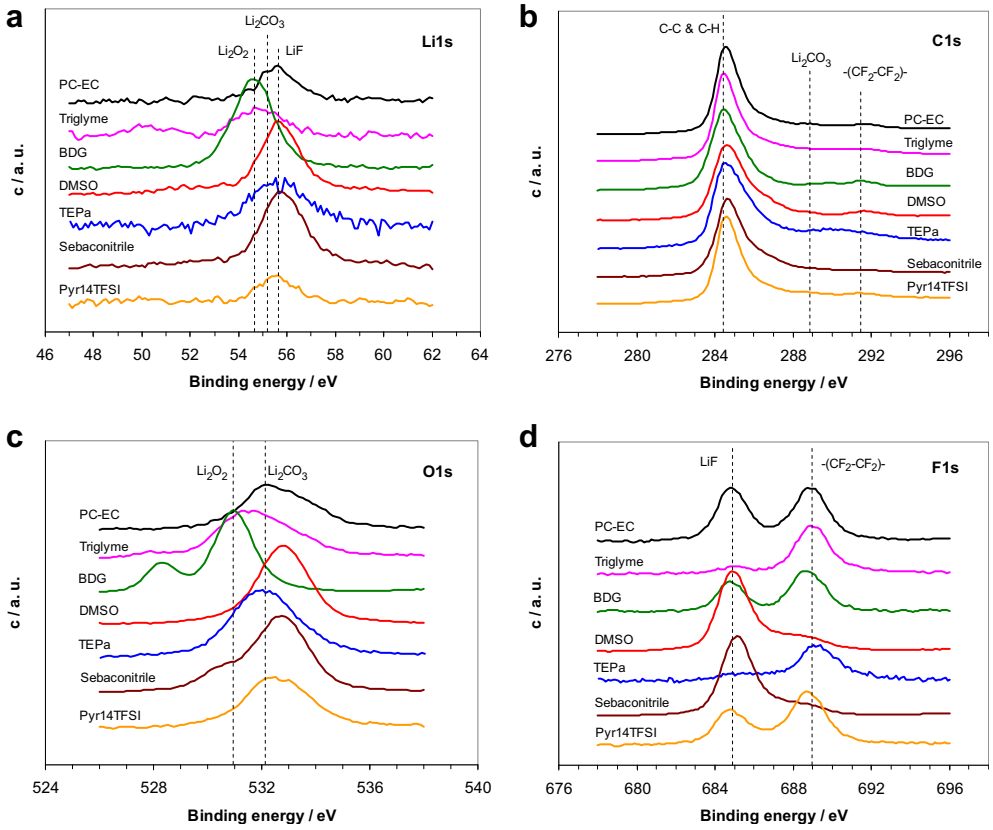

Fig. 3. XPS results of the discharged KB-air electrodes when different electrolyte solvents were used, where the elements are (a) Li1s, (b) C1s, (c) O1s, and (d) F1s.

reversibility is related to the significant formation of LiF, Li_2CO_3 and other byproducts during discharge process, as it is revealed from the above XRD and XPS results. The release of O_2 during charging process of all the discharged air electrodes means that more or less amount of Li_2O_2 was formed in the Li-O_2 cells using all six types of solvents studied in this work, although there are no characteristic peaks of Li_2O_2 in the XRD patterns of the air electrodes discharged in several electrolytes, which is because of the low content or poor crystallinity of the formed Li_2O_2.

The discharge products in the KB-air electrodes were further analyzed using the solid-state ^{13}C MAS NMR technique. Fig. 5 illustrates the solid-state ^{13}C MAS NMR spectra of the washed discharged electrodes. The characteristic peak of carbon for Li_2CO_3 is located at ca. 169 ppm, and the peak at ca. 112 ppm is attributed to the Kel-F signal from the two end plugs inside the MAS rotor. Notably, Li_2CO_3 is formed in all the air electrodes during discharging from all the electrolytes studied, as demonstrated from the above XRD and XPS results. A quantitative calculation of the Li_2CO_3 signal was conducted based on the weight of the air electrode and the total number of scans on the Li_2CO_3 signal. The values are listed in Fig. 5 for each of the solvents. The higher value of Li_2CO_3 signal per mg electrode and per scan means more Li_2CO_3 exists in the air electrode. It is seen that BDG leads to the least amount of Li_2CO_3 among the studied solvent systems, and Sebaconitrile is the second best solvent to form less Li_2CO_3. It is interesting to see that the carbonate electrolyte is not the worst to form Li_2CO_3. Contrarily, Triglyme, Pyr14TFSI and DMSO are the solvents that result in significantly high content of Li_2CO_3 during discharging. In recent work, we demonstrated that Li_2CO_3 cannot be oxidized during the charging process up to 4.5 V [17]. The formation of Li_2CO_3 during the discharge process of a Li-air battery indicates that this battery will have a low Coulombic efficiency and a short cycle life. In other words, even the glyme-based electrolytes are not feasible for rechargeable Li-air batteries with long cycle life.

To examine how Li_2CO_3 is formed in glyme-based electrolytes (i.e., to investigate whether the Li_2CO_3 is produced by the carbon electrode or by the electrolyte), we used ^{13}C isotope-enriched carbon (99%, from Sigma–Aldrich) to prepare the ^{13}C-labeled air electrode. The battery was discharged in the same electrolyte (1.0 M LiTFSI in Triglyme) in an oxygen atmosphere. The hypothesis is that, if Li_2CO_3 comes from the carbon electrode, the ^{13}C MAS NMR signal corresponding to Li_2CO_3 would increase by more than ninetyfold using 99% ^{13}C labeling, because the natural abundance of ^{13}C is only 1.1% without isotope enrichment. Fig. 6 shows the ^{13}C MAS NMR spectrum of the discharged ^{13}C-labeled air electrode in unwashed and washed states compared with that of the discharged regular KB-air electrode in a washed state. Obviously, the signal of Li_2CO_3 in the unwashed and washed ^{13}C-labeled carbon electrodes is not larger than the corresponding signals in the natural carbon electrode. This result unambiguously demonstrates that the Li_2CO_3 originated not from the carbon electrode but from the Triglyme electrolyte. When comparing the ^{13}C MAS NMR spectra of the 99% ^{13}C-labeled electrodes, the peaks between ~60 and ~85 ppm disappear in the washed electrode, indicating that these signals originated from the electrolytes and were washed off during the electrode cleaning process. We believe that during the discharge process the superoxide radical anions attack the alkylene group (CH_2) close to the ether bond (C—O), cause the deformation of the molecules and decompose them into CO_2 or carbonate groups that in turn form Li_2CO_3 by reacting with the simultaneously formed LiO_2 or Li_2O_2. This process has also been demonstrated by Bruce and co-workers [24]. On the other hand, the carbon electrode itself is

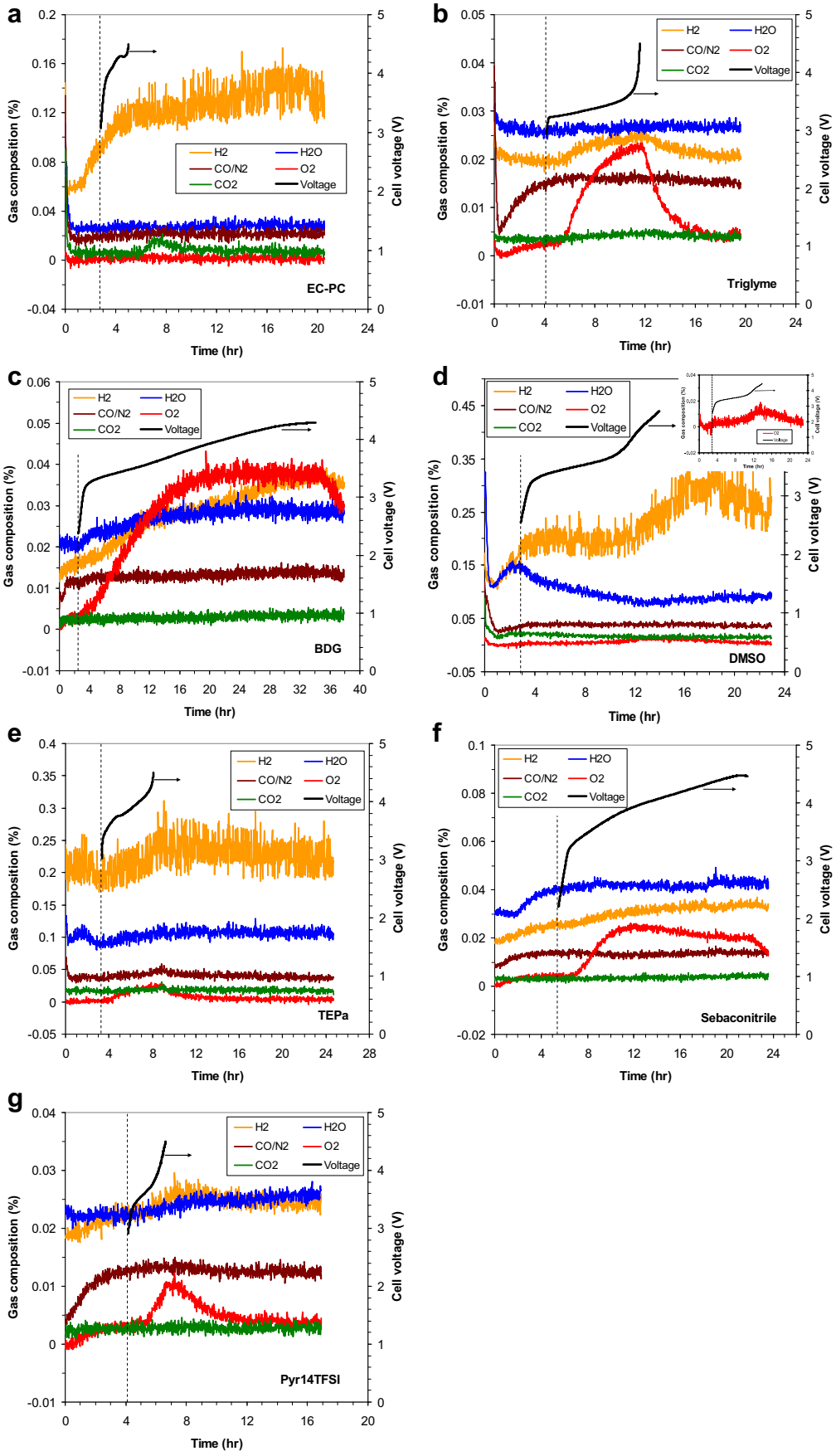

Fig. 4. Gas formation and composition during charge process to the air electrodes discharged in different electrolytes based on (a) PC-EC (1:1 wt). (b) Triglyme, (c) BDG, (d) DMSO, (e) TEPa, (f) Sebaconitrile, (g) Pyr14TFSI, tested by in-situ GC/MS method.

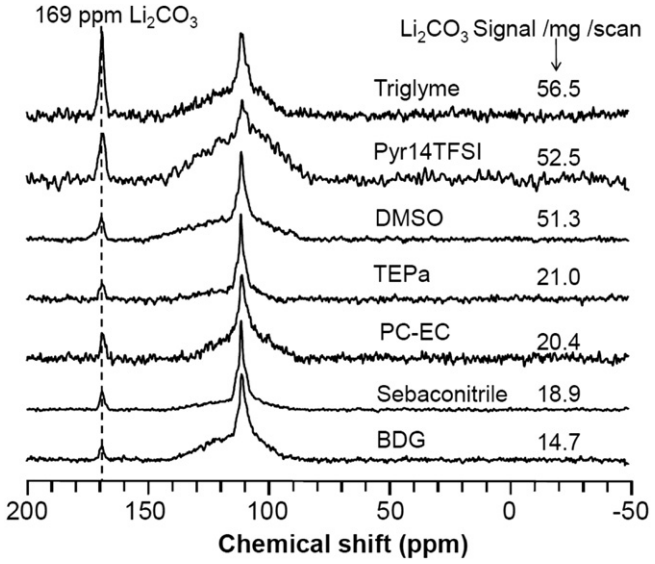

Fig. 5. 500 MHz ^{13}C-MAS NMR spectra of the KB-air electrodes after discharging in different electrolytes with different organic solvents.

stable under the given discharge conditions, and no trace of ^{13}C was observed in Li_2CO_3 formed during the discharge process.

It has been reported that, with carbonate solvents, lithium alkylcarbonates and Li_2CO_3 are the primary discharge products, with a trace amount of Li_2O_2 being formed [12–17]. The superoxide radical anions preferably attack the ethereal carbon atom of carbonate molecules via a nucleophilic reaction to form lithium alkylcarbonates and Li_2CO_3 [16,25]. Bryantsev et al. also used density functional theory (DFT) calculations with a Poisson-Boltzmann continuum solvent model to predict the solvent stability with superoxide radical anion [25]. They reported that the nucleophilic attack of the superoxide radical anion to the aprotic solvents commonly occurs at the single oxygen-carbon bond of carbonates, sulfonates, aliphatic carboxylates, lactones, phosphates and the single bond of sulfur-carbon for sulfones. Such attack then causes the decomposition of the solvent molecules and reactions with other species to finally form Li_2CO_3.

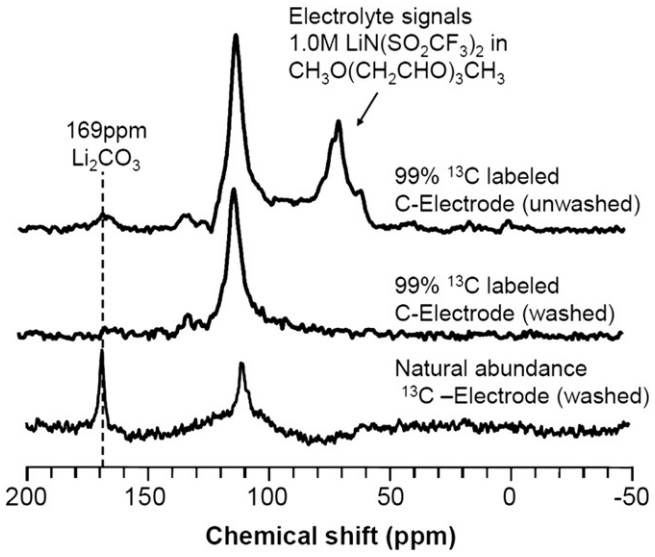

Fig. 6. Comparison of ^{13}C-MAS NMR spectra of the ^{13}C-labeled carbon air electrode and the regular KB-air electrode after discharging in an electrolyte of 1.0 M LiTFSI in Triglyme.

The nitriles with short alkyl chains, such as acetonitrile, are reported to show high electrochemical redox reversibility for superoxide radical anions in tetrabutylammonium salt-based electrolytes [19,25,26], thus indicating good stability when exposed to superoxide radical anions. However, nitriles with short alkyl chains are reactive to lithium metal and have high volatility so they cannot practically be used in Li-air batteries unless the lithium anode is well protected, as in the case of aqueous based Li-air batteries. Sebaconitrile, a nitrile with a long alkyl chain, is relatively stable to lithium metal and has a high boiling point. However, the hydrogen atom on the α-position of the nitriles is chemically unstable against Lewis bases due to its high acidity [27,28]. Therefore, Sebaconitrile also leads to the formation of Li_2CO_3 and LiF besides the desired Li_2O_2 during discharge, as indicated in the above discussed XPS and NMR study. Thus, nitriles are not appropriate solvents for Li-air batteries either.

As discussed above, although a small portion of Li_2O_2 is identified in discharge products when the Li-O_2 battery is discharged in the ionic liquid Pyr14TFSI, the majority of the discharge products are not Li_2O_2. On the other hand, Pyr14TFSI also exhibits high viscosity and relatively low conductivity. Therefore, Pyr14TFSI is not a feasible electrolyte solvent for Li-air batteries.

4. Conclusions

The discharge performances and discharge products of Li-O_2 batteries with different aprotic organic solvents were investigated systematically. The results from XRD, XPS and GC/MS indicate that, among the studied solvents (including carbonate, glymes, sulfoxide, phosphate, nitrile, and ionic liquid), only glymes lead to significant formation of Li_2O_2 (which is desired for reversible Li-O_2 or Li-air batteries) during the discharge process of Li-O_2 batteries, although a small amount of Li_2O_2 was also generated in phosphate, nitrile, ionic liquid, and sulfoxide. However, Li_2CO_3 and LiF are also present in the discharge products of Li-O_2 batteries using all the six types of solvent systems studied, including the glymes (BDG and Triglyme). This has led to significantly reduced Coulombic efficiency and will shorten the cycle life of the Li-air batteries. Less Li_2CO_3 and much higher discharge capacity were found in Li-O_2 batteries using BDG as the electrolyte solvent as compared with those using Triglyme, which makes BDG the appropriate solvent for Li-O_2 batteries among the studied solvents. The ^{13}C MAS-NMR spectrum of the discharged ^{13}C-labeled air electrode unambiguously reveals that Li_2CO_3 is formed from the oxidation of the solvent and not from the oxidation of the carbon based air electrode. The formation of LiF can be attributed to the decomposition of imide salt and/or Teflon binder. Therefore, new electrolyte systems that can ensure the formation of Li_2O_2 on the air electrodes and minimize other reaction products during the discharge process need to be further investigated.

Acknowledgments

This work was supported by the Laboratory Directed Research and Development Program at Pacific Northwest National Laboratory (PNNL), a multi-program national laboratory operated by Battelle for the U.S. Department of Energy (DOE). The XPS measurements were performed at the Environmental Molecular Sciences Laboratory, a national scientific user facility sponsored by the DOE's Office of Biological and Environmental Research and located at PNNL. The authors thank Dr. Dehong Hu of PNNL for the FTIR test and Drs. Jun Liu and Gordon L. Graff of PNNL for their valuable input.

References

[1] C.Ó. Laoire, S. Mukerjee, K.M. Abraham, E.J. Plichta, M.A. Hendrickson, J. Phys. Chem. C 113 (2009) 20127.
[2] R.P. Hamlen, T.B. Atwater, in: D. Linden, T. Reddy (Eds.), Handbook of Batteries, third ed. McGraw Hill, New York, USA, 2001 Ch. 38.
[3] W. Xu, J. Xiao, D. Wang, J. Zhang, J.-G. Zhang, J. Electrochem. Soc. 157 (2010) A219.
[4] J.-G. Zhang, D. Wang, W. Xu, J. Xiao, R.E. Williford, J. Power Sources 195 (2010) 4332.
[5] K.M. Abraham, Z. Jiang, J. Electrochem. Soc. 143 (1996) 1.
[6] J. Read, J. Electrochem. Soc. 149 (2002) A1190.
[7] T. Ogasawara, A. Débart, M. Holzapfel, P. Novák, P.G. Bruce, J. Am. Chem. Soc. 128 (2006) 1390.
[8] A. Débart, J. Bao, G. Armstrong, P.G. Bruce, J. Power Sources 174 (2007) 1177.
[9] A. Débart, A.J. Paterson, J. Bao, P.G. Bruce, Angew. Chem. Int. Ed. 47 (2008) 4521.
[10] H. Cheng, K. Scott, J. Power Sources 195 (2010) 1370.
[11] D. Zhang, Z. Fu, Z. Wei, T. Huang, A. Yu, J. Electrochem. Soc. 157 (2010) A362.
[12] F. Mizuno, S. Nakanishi, Y. Lotani, S. Yokoishi, H. Iba, Electrochem. 78 (2010) 403.
[13] J. Xiao, J. Hu, D. Wang, D. Hu, W. Xu, G.L. Graff, Z. Nie, J. Liu, J.-G. Zhang, J. Power Sources 196 (2011) 5674.
[14] W. Xu, V.V. Viswanathan, D. Wang, S.A. Towne, J. Xiao, Z. Nie, D. Hu, J.-G. Zhang, J. Power Sources 196 (2011) 3894.
[15] B.D. McCloskey, D.S. Bethune, R.M. Shelby, G. Girishkumar, A.C. Luntz, J. Phys. Chem. Lett. 2 (2011) 1161.
[16] S.A. Freunberger, Y. Chen, Z. Peng, J.M. Griffin, L.J. Hardwick, F. Bardé, P. Novák, P.G. Bruce, J. Am. Chem. Soc. 133 (2011) 8040.
[17] W. Xu, K. Xu, V.V. Viswanathan, S.A. Towne, J.S. Hardy, J. Xiao, Z. Nie, D. Hu, D. Wang, J.-G. Zhang, J. Power Sources 196 (2011) 9631.
[18] C.Ó. Laoire, S. Mukerjee, K.M. Abraham, E.J. Plichta, M.A. Hendrickson, J. Phys. Chem. C 114 (2010) 9178.
[19] C.Ó. Laoire, S. Mukerjee, E.J. Plichta, M.A. Hendrickson, K.M. Abraham, J. Electrochem. Soc. 158 (2011) A302.
[20] J. Xiao, D. Wang, W. Xu, D. Wang, R.E. Williford, J. Liu, J.-G. Zhang, J. Electrochem. Soc. 157 (2010) A487.
[21] W. Xu, J. Xiao, D. Wang, J. Zhang, J.-G. Zhang, J. Electrochem. Soc. 156 (2009) A773.
[22] S. Hayashi, K. Hayamizu, Bull. Chem. Soc. Jpn. 64 (1991) 685.
[23] Y. Ein-Eli, A. Kraytsberg, J. Electrochem. Soc. 158 (2011) S13.
[24] S.A. Freunberger, Y. Chen, N.E. Drewett, L.J. Hardwick, F. Bardé, P.G. Bruce, Angew. Chem. Int. Ed. 50 (2011) 8609.
[25] V.S. Bryantsev, V. Giordani, W. Walker, M. Blanco, S. Zecevic, K. Sasaki, J. Uddin, D. Addison, G.V. Chase, J. Phys. Chem. A 115 (2011) 12399.
[26] Z. Peng, S.A. Freunberger, L.J. Hardwick, Y. Chen, C. Giordani, F. Barde, P. Novak, D. Graham, J.-M. Tarascon, P.G. Bruce, Angew. Chem. Int. Ed. 50 (2011) 6351.
[27] J. San Filippo Jr., L.J. Romano, C.-I. Chern, J. Org. Chem. 41 (1976) 586.
[28] Y. Sawaki, Y. Ogata, Bull. Chem. Soc. Jpn. 54 (1981) 793.